

Charting Spatiotemporal Environments with Chained, Open-Loop Trajectories Optimized over Physically-Informed Uncertainty Forecasts

Victoria L. Preston*

Aeronautics and Astronautics
Massachusetts Institute of Technology
Cambridge, MA 01275
vpreston@csail.mit.edu

Genevieve E. Flasphohler*

Electrical Engineering and Computer Science
Massachusetts Institute of Technology
Cambridge, MA 01275
geflaspo@csail.mit.edu

Daniel Yang

Electrical Engineering and Computer Science
Massachusetts Institute of Technology
Cambridge, MA 01275
dxyang@csail.mit.edu

Scott Wankel

Marine Chemistry and Geochemistry
Woods Hole Oceanographic Institution
Woods Hole, MA 02543
sdwankel@whoi.edu

John Fisher III

CSAIL
Massachusetts Institute of Technology
Cambridge, MA 01275
jfisher@csail.mit.edu

Anna P. M. Michel

Applied Ocean Physics and Engineering
Woods Hole Oceanographic Institution
Woods Hole, MA 02543
amichel@whoi.edu

Nicholas Roy

CSAIL
Massachusetts Institute of Technology
Cambridge, MA 01275
nickroy@csail.mit.edu

Abstract

In the environmental sciences, spatiotemporal phenomena are ubiquitous. Robots are uniquely well-suited for environmental exploration and sample collection, however to collect elucidating observations of unknown, partially-observed spatiotemporal distributions for scientific inquiry requires decision-making under typically severe operational constraints. Here, we propose a methodology, PHORTEX, that enabled an autonomous underwater vehicle (AUV) to map volatile deep sea hydrothermal plumes via chained, open-loop trajectory primitives (e.g., lawnmowers) optimized with respect to an information measure computed over physically-informed uncertainty forecasts of environmental dynamics learned from *in situ* observations. In developing this methodology, we address core challenges in developing an autonomy stack that can integrate observations from heterogeneous sensors into a model of a spatiotemporal system, then use this model to plan informative trajectories that targets a specific scientific objective. [TODO: will want a pithy summary of results sections to be included here.]

1 Introduction

Transient, dynamic phenomena—deep-sea hydrothermal plumes, algal blooms, lava flows—are of interest in many disciplines of observational science. Observations and *in situ* samples of these phenomena are necessary for scientific discovery and model development. However, a single, static sensor is often insufficient to develop a comprehensive picture of these spatiotemporal phenomena due to their large spatial scales and dynamic temporal nature. Large networks of static sensor nodes could address this sensing challenge, but the transience and sparsity of the target phenomena would necessitate logically impractical sensor density. By contrast, mobile robots can actively seek and perform targeted surveys of ephemeral phenomena and are uniquely well-positioned for extended deployment carrying heterogeneous sensor payloads.

Robots deployed for *expeditionary science* today often execute open-loop, preset trajectories, like “lawnmowers” (back-and-forth grid-based pattern) hand-designed by human scientists (e.g., [Camilli et al., 2010]). In dynamic environments, this open-loop execution results in sparse measurements of the target phenomena or misses a short-lived target entirely [Flaspohler et al., 2019]. Given the cost of scientific field operations and the value of the data collected, it is critical to improve the efficiency and efficacy of robots as scientific tools.

Building robotic platforms to collect scientific observations of transient, spatiotemporal phenomena requires an autonomy stack that can integrate observations from heterogeneous sensors into a model of a spatiotemporal distribution and use this model to plan informative trajectories that target a specific scientific objective. This kind of autonomy poses many challenges for integrating probabilistic modeling and decision-making. Previous work in informative path planning (IPP) [Hitz et al., 2017], adaptive sampling/experimental design [Krause et al., 2008a], and decision-making under uncertainty [Sunberg and Kochenderfer, 2018] has tackled aspects of the expeditionary science problem, especially in static environments using data-driven models and information-based rewards. However, existing methodologies do not trivially extend to spatiotemporal environments, leaving key challenges such as model and dynamics learning and decision-making in large-scale environments unaddressed.

In this paper, we discuss the algorithmic and operational challenges of deploying robots for expeditionary, sample-collection missions, and present our autonomy stack, PHORTEX: **P**Hysically-informed **O**pen-loop **R**obotic **T**rajectories for **E**Xpeditions, which enables forecasting of spatiotemporal distributions from sparse *in situ* measurements, and optimizes open-loop trajectories that respect the operational constraints of state-of-the-art robotic platforms. We demonstrate PHORTEX for the task of hydrothermal plume charting in the deep sea, and show results from a field campaign in the Guaymas Basin, Gulf of California in November 2021. We conclude with a discussion of **[TODO: pithy summary of discussion section when complete]**.

1.1 Charting Deep Sea Hydrothermalism

Hydrothermal vents in the ocean were first observed in 1977 [Corliss et al., 1979] at the Galapagos Rift, and since have been a concerted focus of a geodynamical and biogeochemical studies. Venting sites can be roughly classified by their proximity to magmatic heat sources from which the fluids emitted from vents are heated (between 20–400 °C compared to a background deep ocean temperature of approximately 2 °C) and imbued with minerals, metals, dissolved gases, and other compounds from which vents get labels of “black smokers” and “white smokers” [Jannasch and Mottl, 1985, Martin et al., 2008]. These warm, nutrient-pumping sites in the deep ocean have created oases of unique micro- and macro-fauna, including perhaps most famously, giant tubeworms [Corliss et al., 1979]. Thus, detection and characterization of seafloor hydrothermal venting are critical for understanding fundamental interactions between the deep ocean, its underlying basaltic crust, the deep biosphere, and (bio)geochemical fluxes.

We build on a wealth of work that has primarily focused on localizing venting plume sources (e.g., [Jakuba, 2007, McGill and Taylor, 2011, Nakamura et al., 2013, Paduan et al., 2018, Mason et al., 2020, Wang et al., 2020, Kim et al., 2020]) and have leveraged ship-based acoustics, towed instrument rosettes, remotely-operated vehicles (ROVs), submersibles, and autonomous underwater vehicles (AUVs). Hundreds of undiscovered vent sites are hypothesized to exist in the deep ocean [Beaulieu et al., 2015] with implications for global nutrient and energy budgets, and novel

ecosystems. Source discovery is a challenging problem given the partial observability of *in situ* equipment, which can distinguish plume-derived fluids from background waters, but fails to resolve the complicated spatiotemporal dynamics of water mixing, tidal advection, water mass mixing, and chaotic turbulence in a series of observations.

We pose a complementary problem: given a discovered venting source, what impact do the venting fluids have on the local environment? Here, rather than use detections of a plume as a means of finding a source, the detections themselves are the valuable data product for scientific inquiry. By placing instruments throughout a plume structure over multiple length- (meter to kilometer) and time- (hours to days) scales to collect dense in-plume measurements, previously unapproachable questions with respect to microbial lifecycle and transport, carbon cycling, and anomalous water mass formation, can be tackled. This problem inherently requires grappling with the same forms of uncertainty as in the source localization problem, in addition to the general challenge of forecasting future states from the only partially observed and unseen dynamics. This is both an *inverse problem*, of extracting the dynamical representation from *in situ* observations, and a *forward problem* of simulating those dynamics into future states in order to plan informative trajectories. In our approach, we explicitly tackle both of these problems in our belief representation framework, which blends a numerical hydrothermal plume model with Bayesian probabilistic representations that can be used to optimize AUV sampling trajectories.

1.2 Expedition Logistics for Deep Sea Robotics

Oceanographic research expeditions require chartering a research vessel that can house scientific teams for weeks at a time, provide workspaces for these scientific and engineering parties, store scientific equipment, facilitate deploying and recovering scientific instruments, withstand variable sea-states, and transit many thousands of kilometers for any given expedition. Undertaking a scientific expedition typically requires coordination and collaboration between different scientific stakeholders, captain and crew aboard a vessel, and external teams that maintain and operate the scientific equipment.

Robotic platforms that are deep sea capable (“deep sea” in this work refers to any depths beyond the mesopelagic zone, over 1000 m) are assets that are requested on an per-expedition basis. A specialized team is typically deployed with the vehicle, responsible for vehicle maintenance and working with the scientific leader to design and execute missions while at sea. Depth-capable AUV assets, like AUV *Sentry* operated by Woods Hole Oceanographic Institution (WHOI) and the National Deep Submergence Facility (NDSF) [Kaiser et al., 2016] used in this study, may be deployed on tens of expeditions each year and operated approximately two-thirds of the year in total. Under these pressures, AUV technologies like *Sentry* are typically flown in fixed survey patterns (e.g., lawnmowers) that can be easily verified before a dive and monitored while underway. Indeed, even rudimentary adaptive behaviors are not inherently possible on many AUVs, although they may be approximated with a shipboard human-in-the-loop to physically issue mission changes while monitoring specialized top-side software external to the AUV computing stack. One of the key difficulties with ship-AUV coordination of this type is the limited communication bandwidth and information transfer that is possible with acoustic modems. Underwater, information transfer cannot happen near instantaneously “over-the-air” like terrestrial networks. Data transfer between AUV and ship to possibly inform adaptive behaviors is limited to a strict subset of all observations at a frequency of 0.02 Hz or less, and issuing complicated or timely motion plans to an AUV from a ship is typically impractical and seldom done. Thus, we assume in this work that AUVs for deep sea research can only be operated in open-loop.

Under these constraints, and the typical working relationship between vehicle engineers and science party as an ad-hoc professional alliance formed only for a singular expedition, the typical workflow for using AUVs by the science party is to provide a set of coordinates and desired survey resolution to vehicle engineers, which translate these requirements into a safe multi-hour survey. At the conclusion of a dive, hours later, data products can be available for review by the science team, and a new plan is generated during vehicle cycling time (on the order of a few hours). Practically, these data products may contain hundreds of thousands of point measurements from multiple heterogeneous sensors. For hydrothermal plume monitoring, a combination of these sensor streams need to be used to make confident plume detections, but information about exact tidal state, state of the venting source, and background sea characteristics requires fusing data products from other instruments deployed on a cruise if available. This makes performing “closed loop” science, in which scientific products directly inform a new mission, operationally challenging at sea, particularly

when designing a new mission requires not just deep analysis of collected data, but forecasting the implications of those observations onto a new day, new site, or new scientific objective. This also ignores the considerable burden of coordinating several other ongoing scientific projects, day-to-day operational changes, and unforeseen discoveries or hurtles.

To this end, our work aims to alleviate the burden of “closing the loop” onboard a research vessel for AUV operations. Situated as a data ingestor, model, forecaster, and planner between AUV dives, our framework generates trajectories that respect operational constraints of the AUV, can incorporate science tasks, intuition, and priors directly into a model, fuse opportunistic data from other instruments/platforms, and display aggregated data products and physically-meaningful estimates for scientific verification. Our autonomy stack and operational suggestions enables both algorithmic and human decision-makers at sea to maximize deployment-by-deployment utility of AUV missions.

1.3 Contributions

In this paper, we present an autonomy stack specifically designed to enable robotic platforms engaged in expeditionary science to intelligently plan open-loop trajectories which honor operational constraints leveraging forecasts of complicated spatiotemporal distributions. Our framework, PHORTEX: **P**Hysically-informed **O**pen-loop **R**obotic **T**rajectories for **E**Xpeditions, introduces a practical-time, sample-efficient iterative mission structure that utilizes a probabilistic model which embeds a simplified scientific description of environmental dynamics to compute uncertainty forecasts and a trajectory optimizer which chains open-loop primitives (e.g., lawnmowers) which maximizes an information reward. We codify the model as PHUMES: **P**Hysically-informed **U**ncertainty **M**odels for **E**nvironment **S**

2 Background and Related Work

2.1 Planning under Uncertainty

In an expeditionary science mission, a robot must make a sequence of decisions in order to collect scientifically useful measurements of an unknown, partially-observable spatiotemporal environment under time, energy, and dynamical constraints. We formulate this sequential decision-making problem as a partially observable Markov decision-process (POMDP). Let $\Pi(\cdot)$ denote the space of probability distributions over the argument. A finite horizon POMDP can be represented as tuple: $(\mathcal{S}, \mathcal{A}, T, R, \mathcal{Z}, O, b_0, H, \gamma)$, where \mathcal{S} are the states, \mathcal{A} are the actions, and \mathcal{Z} are the observations. At planning iteration t , the agent selects an action $a \in \mathcal{A}$ and the transition function $T : \mathcal{S} \times \mathcal{A} \rightarrow \Pi(\mathcal{S})$ defines the probability of transitioning between states in the world, given the current state s and control action a . The transition function governs both how the state of the robot will evolve, given a chosen action, and the potentially stochastic evolution of the underlying spatiotemporal environment.

After the state transition, the agent receives an observation according to the observation function $O : \mathcal{S} \times \mathcal{A} \rightarrow \Pi(\mathcal{Z})$, which defines the probability of receiving an observation, given the current state s and previous control action a . The observation function connects the readings of the robot’s potentially heterogeneous sensor payload to the state representation that is used to represent the spatiotemporal environment. Finally, the reward function $R : \mathcal{S} \times \mathcal{A} \rightarrow \mathbb{R}$ serves as a specification of the task, assigning the states of the world that are useful for a given scientific objective high reward and others low reward. A POMDP is initialized with belief $b_0 \in \Pi(\mathcal{S})$ — an initial probability distribution over state — and plans over horizon $H \in \mathbb{Z}^+$ with discount factor $\gamma \in [0, 1]$.

As the robot moves through the world, it selects actions and receives observations. Because the state of the world is

not directly observable in a POMDP, the robot maintains a probability distribution over possible states — termed a *belief* — and must update this belief each time it takes an action and receives an observation. Given the transition and observation models, the belief can be updated directly using Bayes rule. We define the belief update function as follows:

$$\tau(b_{t-1}, a_{t-1}, z_t) = b_t \triangleq \mathbb{P}(S_t | a_0, z_0, \dots, a_{t-1}, z_{t-1}, z_t) \quad (1)$$

$$= \mathbb{P}(S_t | b_{t-1}, a_{t-1}, z_t) \quad (2)$$

$$= \frac{\int_{s \in \mathcal{S}} O(s, a_{t-1}, z_t) T(s, a_{t-1}, s') b_{t-1}(s')}{\mathbb{P}(z_t | b_{t-1}, a_{t-1})} \quad (3)$$

This equation is known as a Bayes filter [Särkkä, 2013] and is often intractable to compute directly and so an approximate Bayesian inference procedure or filter is used to represent the belief, such as a Kalman filter [Welch et al., 1995], particle filter [Silver and Veness, 2010], or more general Markov Chain Monte Carlo (MCMC) or variational methods.

Due to the stochastic, partially observable nature of current and future states, the realized reward in a POMDP is a random variable. Optimal planning is defined as finding a horizon-dependent policy $\{\pi_t^* : \Pi(\mathcal{S}) \rightarrow \mathcal{A}\}_{t=0}^{H-1}$ that maximizes expected reward: $\mathbb{E} \left[\sum_{t=0}^{H-1} \gamma^t R(S_t, \pi_t(b_t)) \mid b_0 \right]$, where b_t is the updated belief at time t , conditioned on the history of actions and observations. The recursively defined horizon- h optimal value function V_h^* quantifies, for any belief b , the expected cumulative reward of following an optimal policy over the remaining planning iterations: $V_0^*(b) = \max_{a \in \mathcal{A}} \mathbb{E}_{s \sim b}[R(s, a)]$ and

$$V_h^*(b) = \max_{a \in \mathcal{A}} \mathbb{E}_{s \sim b}[R(s, a)] + \gamma \int_{z \in \mathcal{Z}} \mathbb{P}(z | b, a) V_{h-1}^*(\tau(b, a, z)) dz \quad h \in [1, H-1], \quad (4)$$

where $\tau(b, a, z)$ is the updated belief after taking control action a and receiving observation z (Eq. (3)). The optimal policy at horizon h is to act greedily according to a one-step look ahead of the horizon- h value function. However, Eq. (4) is intractable for large or continuous state, action, or observation spaces and thus the optimal policy must be approximated. Much of the art of practical decision-making uncertainty is making well-designed algorithmic and heuristic choices that enable efficient and robust planning algorithms.

2.2 Bayesian Inverse Problems

Belief representations utilized for approximating solutions for POMDPs are typically expressed as Bayesian models in order to perform inferences over a set of unknown parameters given a set of observations. Specifically, a Bayesian inference problem takes the following form: let $\mathcal{X} = X_0, \dots, X_{N-1}$ be a set of N random variables with a joint distribution $\Pr(X_0, \dots, X_{N-1})$. A subset of these random variables are observed, \mathcal{X}_{obs} ; latent variables are those that are not observed $\mathcal{X}_{\text{lat}} = \mathcal{X} \setminus \mathcal{X}_{\text{obs}}$. Bayes Theorem lets the subset of observed variables to inform the latent:

$$\Pr(\mathcal{X}_{\text{lat}} | \mathcal{X}_{\text{obs}}) = \frac{\Pr(\mathcal{X}_{\text{lat}}, \mathcal{X}_{\text{obs}})}{\Pr(\mathcal{X}_{\text{obs}})} = \frac{\Pr(\mathcal{X}_{\text{lat}}, \mathcal{X}_{\text{obs}})}{\sum_{\mathcal{X}_{\text{lat}}} \Pr(\mathcal{X}_{\text{lat}}, \mathcal{X}_{\text{obs}})} \quad (5)$$

Practically, computing the denominator (the marginal likelihood of the observations) is computationally expensive, and so approximation techniques like variational Bayesian inference or Monte Carlo (MC) inference methods [MacKay, 1998] may be employed. In this work, we make use of MC methods to estimate the true posterior $\Pr(\mathcal{X}_{\text{lat}} | \mathcal{X}_{\text{obs}}) \sim p(\theta | y)$. Approximate estimators (Φ) of a function $\phi(\cdot)$ with respect to the true density $p(y)$ are computed by drawing samples from a proposal density $q(y)$ and those samples are evaluated with respect to $p(y)$ in order to approximate Φ . MC methods generally require that the form of $q(y)$ lie near the form of $p(y)$. In large, complex systems, it is difficult to define a single density that captures these characteristics. Markov chain MC (MCMC) algorithms address this by drawing samples using a proposal density which relies on the state of the previous sample, and an acceptance ratio is computed to transition between states [MacKay, 1998, Green, 1995, Neal et al., 2011]. In all MCMC samplers, because each new state relies on a density informed by the previous state, a “burn-in” period, in which a potentially large number of samples are drawn, is necessary before virtually independent samples are generated. MC methods will converge to the true estimator of the posterior [MacKay, 1998] for large numbers of samples.

2.3 Generalized, Analytical, and Numerical Plume Models

Hydrothermal plumes in the deep sea are typically characterized as buoyancy-driven water masses. On formation at a vent site, emitted fluids are significantly less dense than background seawater (by virtue of being super-heated, with some add-on effects by changes in chemical composition). This less dense water mass rise rapidly in the water column, forming a *buoyant stem*, which as a rule of thumb grow in diameter about 1 m for every 10 m vertically travelled. Due to rapid cooling, turbulent mixing, and the natural stratification of ocean water, vent-derived waters will reach a point of neutral-buoyancy with the background seawater. At this point, the plume forms a *nonbuoyant or neutrally buoyant layer* which spreads out across the isopycnal that describes the ocean layer of equivalent density. In the Atlantic basin, plume rise height is typically expected to be approximately 300-350 m; in the Pacific basin, this is 150-200 m [Speer and Rona, 1989]. This buoyant stem and neutrally-buoyant layer model of a hydrothermal plume has been mathematically codified perhaps most famously by [Morton et al., 1956] as a system of conservative equations (here for a stratified fluid) in cylindrical coordinates (x, r) with the x -axis vertical with the vent source at the origin:

$$\text{Volume: } \frac{d}{dx}(b^2 u) = 2b\alpha u \quad (6)$$

$$\text{Momentum: } \frac{d}{dx}(b^2 u^2) = 2b^2 g \frac{\rho_o - \rho}{\rho_1} \quad (7)$$

$$\text{Density deficiency: } \frac{d}{dx}(b^2 u g \frac{\rho_o - \rho}{\rho_1}) = 2b^2 u \frac{g}{\rho_1} \frac{d\rho_o}{dx} \quad (8)$$

where α is a proportionality coefficient which represents gross mixing (or entrainment) that occurs at the edge of a plume, $b = b(x)$ is the (symmetric) radius of the plume, $\rho = \rho(x, r)$ is density inside the plume, $\rho_o = \rho_o(x)$ is density outside of the plume, and ρ_1 is some reference density such that $\rho_o(0) = \rho_1$, and $u = u(x, r)$ is vertical velocity. These equations have been equivalently expressed in terms of mass, salt, heat, and momentum conservation by [Speer and Rona, 1989] which usefully decomposes density into components of salinity and temperature which can be directly observed by instruments.

In most environments, advective cross-flow is present. This “bends” a buoyant stem and reduces the effective rise height of the plume by introducing more aggressive mixing. To describe the plume shape under crossflow, we make use of a model introduced by [Tohidi and Kaye, 2016] described here with respect to a coordinate system of along a modified cylindrical coordinate system with an along-center axis s and centerline trajectory angle θ :

$$\frac{dQ}{ds} = Q \sqrt{\frac{2(1 + \lambda^2)}{M\lambda}} (\alpha \left| \frac{M}{Q} - U_a \cos \theta \right| + \beta \left| U_a \sin \theta \right|) \quad (9)$$

$$\frac{dM}{ds} - U_a \cos \theta \frac{dQ}{ds} = \frac{FQ}{M} \sin \theta \quad (10)$$

$$U_a \sin \theta \frac{dQ}{ds} + M \frac{d\theta}{ds} = \frac{FQ}{M} \cos \theta \quad (11)$$

$$\frac{dF}{ds} = -QN^2 \sin \theta \quad (12)$$

$$x = \int_0^s \cos \theta ds \quad (13)$$

$$z = \int_0^s \sin \theta ds \quad (14)$$

where $U_a = U_a(z)$ is the ambient crossflow velocity, $Q = Q(s, \theta)$ represents the plume specific volume flux, $M = M(s, \theta)$ is the specific momentum flux, $F = F(s, \theta)$ is specific buoyancy flux, N is the Brunt-Vaisala frequency, and α and β are vertical and horizontal entrainment coefficients.

These derived models describe a physically-informed envelope in which plume-derived masses, on average, will be observable under consistent environmental conditions in time (that is, they are spatially-averaged models). Numerical models which can capture instantaneous, complicated structure of plume phenomenon in time [Lavelle et al., 2013, Xu and Di Iorio, 2012] have been developed which enhance the conservative models by directly modeling partial derivatives with respect to time, and incorporating additional dynamical models such as the Navier Stokes equation.

Finally, generalized plume models which have been commonly incorporated in robotic source seeking literature, include the Gaussian plume model [Green et al., 1980], and the Gaussian puff model [Ludwig et al., 1977]. These models primarily describe the dispersion envelope of aerosols released as a plume from a coherent source, modeling the concentration of those aerosols directly as a Gaussian around the centerline describing the plume shape. These models have largely been used in atmospheric contexts to model ground pollution characteristics of smoke-stack like sources, and further typically assume that the advective crossflow (which can be variably modeled in time in the Gaussian puff model) dominates plume movement. Both of these assumptions (the smokestack in a flat world with essentially no stratification, and dominant advection) are broken in the deep sea, which is stratified, typically weakly advected, and with plumes that are significantly buoyant.

2.4 Informative Path Planning

Informative path planning (IPP) is a broad technical field which develops adaptive sampling frameworks for mobile platforms which optimizes trajectories over informative metrics. Several common information measures in environmental sensing applications include:

- Upper-Confidence Bound (UCB) [Agrawal, 1995, Auer, 2002, Snoek et al., 2012] of the form $R_{UCB} = \mu(\mathbf{x}) + \sqrt{\beta\sigma(\mathbf{x})}$ which is the sum of predictive mean μ and variance σ at queries \mathbf{x} . UCB is submodular [Nemhauser et al., 1978].
- Probability of Improvement (PI) [Snoek et al., 2012, Kushner, 1964]; a probability measure of whether a query \mathbf{x} will be better than the current best measurement \mathbf{x}^* .
- Expected Improvement (EI) [Snoek et al., 2012, Jones et al., 1998]; a measure of how much better a proposed query \mathbf{x} will be compared to the current best measurement \mathbf{x}^* .
- Predictive Entropy Search (PES) [Hennig and Schuler, 2012, Hernández-Lobato et al., 2014]; a measure of the conditional entropy between a query \mathbf{x} and a predicted optimizer of a distribution $f(\cdot)$, \mathbf{x}^* .

IPP decision-making frameworks can be offline or online. Canonical offline IPP techniques for pure information-gathering that optimize submodular coverage objectives (e.g., UCB) can achieve near-optimal performance [Srinivas et al., 2012, Binney and Sukhatme, 2012]. Adaptive or online IPP techniques can make use of discrete state spaces [Lim et al., 2016, Arora et al., 2017], known metric maps [Singh et al., 2009, Jawaid and Smith, 2015], unconstrained sensor placement [Krause et al., 2008b], or nonmyopic sensor placement [Flaspohler et al., 2019] in order to design trajectories through a potentially large state and vehicle space in order to gather useful observations. In this work, we utilize UCB within our trajectory optimization procedure.

2.5 Plume Hunting with Robots

In the robotics literature, plume hunting has been equivalently styled as odor mapping, odor localization, source localization, and source seeking. In a large portion of these works, it is assumed that the source *location* is unknown, and through partial observations of emitted gas/odor/plume, the source can be discovered using techniques that can be divided broadly into biologically-inspired heuristic search (e.g., [Reddy et al., 2022, Chen and Huang, 2019]) or adaptive informative path planning (e.g., [Salam and Hsieh, 2019, Jakuba, 2007]). Biologically-inspired or heuristic techniques draw (varying-levels of) inspiration from animal or insect behavior in olfactory settings. Such techniques typically include gradient-based algorithms like chemotaxis [Morse et al., 1998], or bio-inspired algorithms that directly mimic

a particular animal [Edwards, 2001]. These techniques are typically reactive and myopic, although they have been demonstrated to be relatively robust in open-world settings. In contrast, adaptive informative path planning can be nonmyopic, and typically attempts to embed knowledge (either heuristically or rigorously) about plume structures to assist in plume localization. Such techniques live on a spectrum, from algorithms that resemble biologically-inspired techniques like infotaxis [Vergassola et al., 2007] to methods that use model order reduction techniques (like proper orthogonal decomposition) to encode complex numerical models (like Navier-Stokes) and elucidate spatiotemporal structures in complex data [Peng et al., 2014]. Some examples of localizing hydrothermal plumes are presented in [Jakuba, 2007, Branch et al., 2020, Wang et al., 2020, Ferri et al., 2010].

In contrast to vent or source localization work, this paper aims to maximize time in a moving plume in order to take samples of the plume trail. Indeed, the plume source is generally known. Work that has used robotic vehicles to map or chart a plume structure has been presented as the “front-tracking” problem [Li et al., 2014]. In this problem, two water masses converge (say, at a river output into a bay), and the goal is to use a robotic vehicle to track the edge or intersection of these water masses. With respect to tasking robots to stay within a water mass, most work has been in demonstrations with multi-robot systems, which identify key “neighborhoods” for examination [Chen and Huang, 2019].

3 Problem Description

Our objective is to map the structure of a time-varying hydrothermal plume using a dynamically constrained AUV and its suite of scientific sensors. This map of a spatiotemporal plume phenomena will enable scientists to infer relevant scientific properties (e.g., chemical flux and transport), as well as to develop and refine models of deep-sea hydrothermal plumes in crossflow environments.

3.1 Types of Closed-loop Autonomy

There are several levels at which an AUV can behave autonomously. At the lowest level, the AUV is given navigation waypoints and executes a closed-loop controller and state estimator to drive to that waypoint; this type of autonomy is commonly implemented and executed on AUV platforms. More sophisticated autonomy systems that are aware of a scientific objectives can build upon these waypoint controllers to enable sophisticated autonomous behavior.

One level up is what we will call *underway* autonomy: after a waypoint is reached, an autonomy stack chooses the next waypoint for a vehicle to target. When operating with underway autonomy, the AUV can act in closed-loop, using observations of the environment in real-time to inform subsequent waypoints while underway. Underway autonomy has the potential to greatly increase the utility of the collected data. For example, the AUV may serendipitously encounter plume water while navigating to a waypoint; an underway autonomy system could then attempt to follow chemical gradients to the plume center. However, there are downsides to underway autonomy, both practical and due to human factors. First, underway autonomy requires that both model updates and planning are run on the robot itself. This quickly leads to computational challenges when models are represented by expensive dynamical simulators and planners necessitate expensive state rollouts. Second, while an AUV is underway, scientists are only able to communicate with the vehicle over low-bandwidth, high latency acoustic links. This leads to serious safety concerns; if the vehicle makes a poor decision and sets an unsafe waypoint, it can take several minutes for that information to be communicated with the ship and for mediating actions to be taken. Therefore, there is significant hesitancy from scientists and engineers alike to enable underway autonomy and the bar to show that an algorithm is safe and trustworthy is incredibly high.

The focus of this paper will instead be on *deployment-by-deployment* autonomy. Unlike underway autonomy, deployment-by-deployment autonomy does not modify the AUV trajectory in real-time while it is underway. In most robotic science missions, an AUV will be deployed in a sequence of dives. While underway on a single dive, the AUV will be constrained to execute an open-loop trajectory that was chosen before the dive. This pre-planned trajectory can undergo a rigorous set of safety checks before vehicle deployment and scientists can examine and validate the planned

trajectories. Then, between dives, the data collected on the previous dive can be used to update a model of the environment and inform the subsequent dive. Model updates and planning can be done with high-power computers on a ship or field station; the robot itself only needs to execute the planned trajectory. Although deployment-by-deployment autonomy is less flexible and reactive than underway autonomy, it is a very useful and practical form of autonomy for many applications of scientific robots.

This closed-loop, deployment-by-deployment decision-making is the focus of the remainder of the paper and our field deployment.

3.2 Deployment-by-Deployment Autonomy as a POMDP

The state space \mathcal{S} The state space of the plume-mapping POMDP consists of the joint state of the environment (i.e., the plume) and the robot. The environment state will be represented by a d -dimensional vector of continuous plume parameters $\mathbf{x}_p \in \mathbb{R}^d$ and a current vector $\mathbf{x}_c \in \mathbb{R}^2$ that contains the heading and velocity of the prevailing crossflow. Finally, the robot state will be represented by a vector $\mathbf{x}_r \in \mathbb{R}^3$ that represents the latitude, longitude, and depth of the robot.

The action space \mathcal{A} The action space of the plume-mapping POMDP will consist of sequences of parameterized lawnmower trajectories (see Fig. 2). This is a constraint given by the AUV operators. Although the AUV is able to execute continuous control actions, the planner was constrained to select parameterized lawnmower trajectories. Multiple lawnmower trajectories could be executed in sequence on a dive to enable a more flexible action set. We assume the a trajectory object is parameterized by a set of real-valued parameters $\theta \in \Theta \subseteq \mathbb{R}^b$. The robot’s action set then consists of sequences of parameterized trajectories, i.e., $\mathcal{A} = \Theta^n$, $n \in \mathbb{Z}^+$.

The transition function T The transition function $T(s, s', a)$ will be decomposed into a plume transition T_p , a current transition T_c , and a robot transition function T_r .

- The plume state parameters \mathbf{x}_p , e.g., plume exit velocity, temperature, are assumed to be constant and therefore the plume transition function T_p is given by: $T_p(\mathbf{x}_p, \mathbf{x}'_p, a) = \delta_{\mathbf{x}_p=\mathbf{x}'_p} \forall a \in \mathcal{A}, \mathbf{x}_p, \mathbf{x}'_p \in \mathbb{R}^d$. Although it is possible for plume parameters to vary on a timescale relevant to a robotic deployment (over the course of hours [Chevaldonné et al., 1991]), the overall impact to gross features of plume rise height, bend angle, and expressed size is essentially negligible.
- The current transition function T_c is more complex and driven by tidal cycles, local bathymetry, and deep sea currents. We will learn the current transition function from current sensor observations by fitting a Gaussian process to model the current time dynamics. This is discussed in detail in Section 6.1.3.
- The robot transition function T_r assumes that the robot’s waypoint controller is deterministically able to execute a planned trajectory: $T_r(\mathbf{x}_r, \mathbf{x}'_r, a) = \delta_{\mathbf{x}'_r=g(\mathbf{x}_r, a)}$, where the function g evaluates the goal waypoint of the trajectory given by a . Although there is some uncertainty in the robots transition, in practice in our field application, localization and control were well solved problems and robust and uncertainty contributed minimally to the robot’s task execution compared with uncertainty about the plume state.

The reward function R The reward function for the plume-mapping POMDP should encode the robot’s objective of producing a comprehensive map of the plume. We choose to approximate this objective by rewarding the robot for collecting observations of “plume water”, i.e., water that is within the plume envelope produced by our analytical plume model $R([\mathbf{x}_p, \mathbf{x}_c, \mathbf{x}_r]^\top, a) = \mathbb{I}[\text{in_plume}(\mathbf{x}_p, \mathbf{x}_r, a)]$ (see **[TODO: we should make some pomdp system figure]**). This heuristic encouraged the robot to align its lawnmower trajectories with the the plume envelope and placing constraints on the minimal size of the a lawnmower trajectory ensured that a diversity of in-plume and out-of-plume samples were collected. Although this is greatly simplified heuristic reward function, it comparatively inexpensive to compute compared to some information theoretic rewards, that would more directly measure uncertainty reduction in, e.g., plume parameters, and worked well in practice. Further, because of the severe constraint requiring the use of

lawnmower primitives, the use of this reward function does not severely reduce the collection of notionally “diverse” samples of plume expression which might be uncertain according to the model.

The observation space \mathcal{Z} The robot carries a variety of scientific sensors, including temperature, salinity, oxidation-reduction potential, optical backscatter, and a novel methane sensor. We developed a sensor model that abstracted these complex scientific observations to a binary measurement of in-plume or out-of-plume (see Section 4.1). Therefore, the observation space of the robot is the set of vector-valued binary observations: $\mathcal{Z} = \{0, 1\}^n, n \in \mathbb{Z}^+$.

The measurement function O The measurement function encodes the complex relationship between the plume parameters, prevailing current, and robot state and the heterogeneous scientific sensors on the robot, each with their own complex sensor physics. Our measurement function consists of two pieces: 1) an analytical plume model, that solves the forward problem, mapping plume parameters \mathbf{x}_p and current state \mathbf{x}_c to a realized plume envelope (see Section 4.2), and 2) a binary pseudo-sensor, which uses a sliding window anomaly detection algorithm to fuse signals from the heterogeneous sensing payload into binary plume detections.

The horizon H and discount factor γ In deployment-by-deployment autonomy, the horizon H can be set to be equal to the number of dives and the discount factor γ set to 1.0. However, an important approximation we make in our specific deployment-by-deployment autonomy problem is that the state of the robot at the end of Dive 1 has little or no impact on its achievable reward in Dive 2 and subsequent dives. This assumption has the impact of setting $\gamma = 0$ and breaks the finite-horizon sequential decision making problem into a sequence of horizon-1 planning problems. The consequences of this assumption may or may not be reasonable in applications of deployment-by-deployment autonomy. It reduces the robots capacity to reason about long-term, multi-dive information gathering actions, for example. However, there are significant computational benefits of performing only single-stage planning and in our hydrothermal plume application, the assumption was reasonable, as the robot was constrained to return to the stationary ship at the end of each dive for recovery and recharging.

4 Methodology

To tackle the core challenge of solving the expeditionary POMDP that we’ve described, we present PHORTEX, which leverages a physically-informed probabilistic method that generates forecasts of spatiotemporal distributions from a history of sparse point observations (PHUMES), and uses a trajectory optimizer which chains open-loop primitives (e.g., lawnmowers) which respect operational constraints in order to maximize an informative reward over these forecasts. PHORTEX is designed to operate iteratively; that is, the robot will operate in a larger “closed-loop” cycle of planning, executing, reporting, planning and so will update it’s forecasts from bulk observations collected in order to inform the next mission (Fig. 1).

4.1 Sensor Modeling

As discussed in Section 3, AUV *Sentry* carries an extensive payload of scientific sensors: salinity, temperature, oxidation-reduction potential (ORP) which measures the relative “reactivity” of water, optical backscatter (OBS) which measures turbidity, oxygen, and dissolved methane. Each of these sensors has it’s own physical characteristics and response to the chemistry of plume water. For example, ORP exhibits a large negative spike when first encountering plume water and then a slow hysteresis back to nominal values. Measurements of salinity, temperature, and oxygen are expected to be influenced not only by plume water, but background physical mixing in the ocean; in contrast, turbidity, ORP, and methane are signals strongly associated with hydrothermalism because they are not persistent in typical seawater. To provide a coherent observation of the presents of plume water, we process these sensor data in two steps: 1) signal processing, and 2) sensor corroboration and binary detection.

In Step 1, we selectively perform four possible steps of processing to each sensor data stream: a) depth-correction, b) log-transform, c) first-differencing, and d) low-pass filtering. *GF: maybe some table with which steps were applied to*

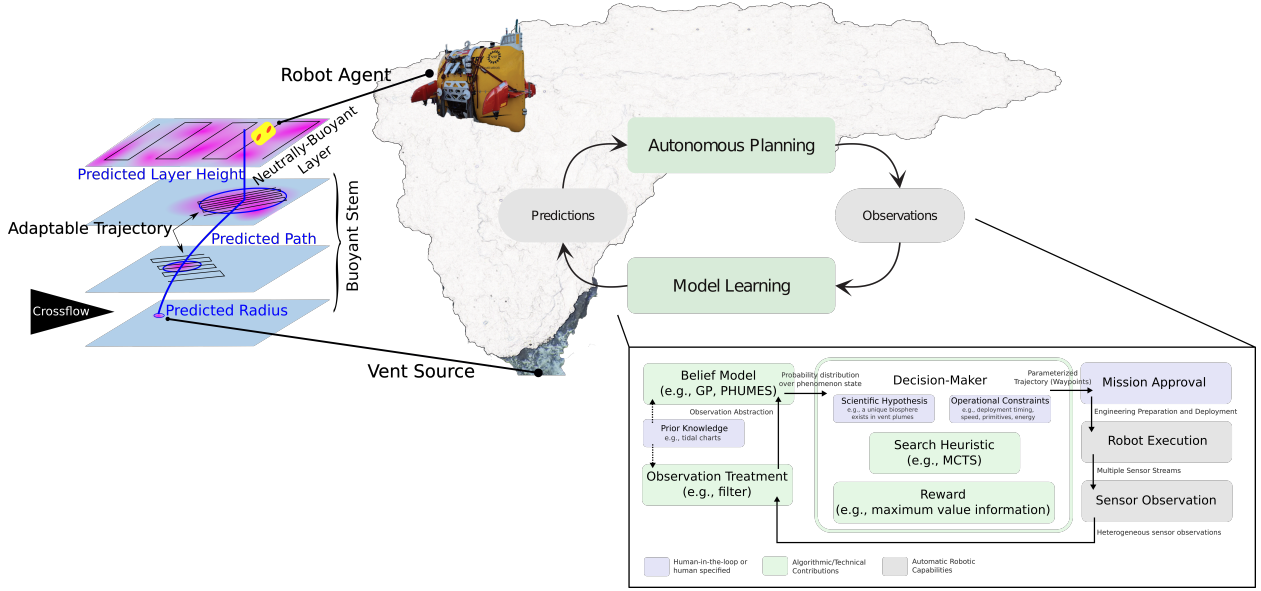


Figure 1: Overview of PHORTEX for hydrothermal plume charting. A robot agent is deployed near a vent source producing hydrothermal fluid which is advected, turbulently mixed, and diffused into the environment. A model of the plume trajectory forms a prediction about the distribution of these fluids, which is used to inform a trajectory optimization scheme which designs a chain of lawnmowers for the robot to execute. After the robot executes this trajectory and gathers in situ observations, these observations are transformed into a binary signal for “in” versus “out” of plume measurements. This signal is used to update the predictive model, used to plan a new mission, and the vehicle is re-deployed.

each sensor stream VP: note that this is subject to change. In Step 2, we take the processed data streams and perform anomaly detection on each individual sensor to identify potential plume water observations. We then use a windowed corroboration method to perform binary detection of plume water: if at least s sensors of S total sensors within a given window W report an anomalous observation, the window is labeled as a positive plume detection. This approach for processing complex sensor observations into binary plume detections was developed by [Jakuba, 2007]; our method is largely based on the process and recommendations provided in this previous work.

The result of our sensor model is to convert multiple, time-stamped sensor observations $s_{t,i} \in \mathbb{R}$, $i = 1, \dots, S$ to a single, binary plume-detection $z_t \in \{0, 1\}$. These binary plume detections are then used to update our plume model and plan robot trajectories, as described in the following sections.

4.2 PHUMES: Physically-informed Uncertainty Forecasts

PHUMES is a model class that can generate predictions of the distribution of a spatiotemporally evolving state given an initial condition and sparse state-space observations. Unlike in typical reinforcement learning methods, the total number of iterations (trials) will be exceedingly small for “training” PHUMES—on the order of 1-3 iterations—and so care must be taken in designing the learner to fully leverage each mission. To overcome extreme partial observability requires embedding some *structure* to the probabilistic representation. For instance, Gaussian Processes (GPs) [Browne et al., 2012], define a kernel function which encodes the relatedness of observations to reduce uncertainty in larger regions of the exploratory state-space than those regions composed only by the observations themselves. GPs are particularly popular in robotic information gathering tasks [Srinivas et al., 2012, Marchant et al., 2014] for this property, however, defining good kernel functions is challenging in non-stationary or spatiotemporal environments [Garg et al., 2012] and GPs are poor extrapolators (i.e., they fail to predict future states effectively).

Instead, PHUMES leverages access to analytical scientific simulators of spatiotemporal phenomenon codified by sys-

tems of ordinary differential equations (ODEs) in order to impart the structure that can be used to overcome sparse observations. These simulators reduce the dimensionality of the inference problem from the full-state of the environmental phenomenon (typically a 4D volume in space and time with continuous phenomenon measurement) to the dimensionality of the initial conditions of the simulator, and are definitionally forward simulators from an initial condition. The use of ODE systems, as opposed to high-fidelity numerical simulators of partial differential equations (PDEs) is intentional; the computational requirement of most PDE systems used to model environmental phenomenon at the scales studied during expeditionary missions is practically intractable. In contrast, ODE systems are less well-resolved, but summarize the structure of an evolving phenomenon in a useful way that can be enhanced by a generic probabilistic formulation wrapping the ODEs.

Within the plume charting POMDP defined, PHUMES generates predictions of the location of plume waters $f(\mathbf{x}_p, \mathbf{x}_c, \mathbf{x}_r | \mathbf{x}_z)$ from the set of continuous plume parameters \mathbf{x}_p , current parameters \mathbf{x}_c , and robot location \mathbf{x}_r given historical *in situ* point detections \mathbf{x}_z and makes use of the system of equations defining a plume in crossflow as defined by [Tohidi and Kaye, 2016] and presented in Section 2.3. In practice, PHUMES consists of a forecasting step (forward simulation) which produces environmental predictions that can be used by the trajectory optimizer to compute the reward function $R([\mathbf{x}_p, \mathbf{x}_c, \mathbf{x}_r]^T, a)$ used by the trajectory optimizer, and an updating step (inverse solution) which updates \mathbf{x}_p from historical observations \mathbf{x}_z . Note that this implies that \mathbf{x}_p is a set of random variables, with prior distribution $\mathcal{P}(\mathbf{x}_p)$ and posterior $\mathcal{P}(\mathbf{x}_p | \mathbf{x}_z)$. With no loss of generality, each of the plume, current, and robot states can be represented as random variables.

In the forecasting step, samples from \mathbf{x}_p which describes physically-meaningful initial conditions (e.g., vent area) and environmental characteristics (e.g., mixing coefficient), \mathbf{x}_c which describes temporal functions (e.g., tidal magnitude), and \mathbf{x}_r which describes robot position are sampled and “pushed through” the crossflow-plume model in order to generate a composite series of snapshots of the spatiotemporal distribution of plume fluids over a query time window. Practically, random samples are drawn over \mathbf{x}_p and \mathbf{x}_c , and a uniform grid or specific query points are drawn for \mathbf{x}_r . This series of snapshots yields a mean and variance at every space-time point defined in \mathbf{x}_r , which can be used to compute the reward function of the trajectory optimizer, which can take the form of a simple informative measure, like UCB. Fig. [TODO: make this] shows an example of a composite snapshot.

Once a mission has been executed and *in situ* measurements collected and transformed into direct (i.e., binary) observations of plume structure, we can update the distributions over the generating initial conditions and parameters \mathbf{x}_p . We use a random-walk Metropolis-Hastings MCMC method [Metropolis et al., 1953]. Simulations of missions through forecasts generated by samples of \mathbf{x}_p pushed through the crossflow plume model are compared with the true observations, and those samples are stochastically accepted or rejected, weighted by agreement between simulated and true observations. As this is a chaining procedure, the next sample is informed by the last, and with enough samples, the distributions are guaranteed to converge to the true underlying distributions.

4.3 Trajectory Optimization for Path Planning

To solve the plume mapping sequential decision-making problem, we begin with the POMDP value function shown in Eq. (4) and introduce the model defined in Section 3:

$$V_h^*(b) = \max_{\{\theta_1, \dots, \theta_n, n | \theta_i \in \Theta, n \in \mathbb{Z}^+\}} \mathbb{E}_{[\mathbf{x}_p, \mathbf{x}_c, \mathbf{x}_r]^T \sim b} [R([\mathbf{x}_p, \mathbf{x}_c, \mathbf{x}_r]^T, \{\theta_1, \dots, \theta_n\})] \quad h \in [0, H-1], \quad (15)$$

where $\theta \in \Theta$ parameterize individual trajectories in a length- n sequence of chained trajectories and b is the planner’s belief about the state of the plume, currents, and robot, and the discount factor γ has been set to zero to encode our single-dive planning approximation. Solving Eq. (15) still involves the challenging optimization over the number n of chained trajectories and the joint optimization of all n trajectories. To further simplify the planning problem, given the constraints of real-world robotic deployments, we assume that the number of chained trajectories is given, i.e., $n = N$, and that each trajectory can be optimized independently. This results in the following approximation:

$$V_h^*(b) \approx \max_{\theta_1 \in \Theta} \dots \max_{\theta_N \in \Theta} \mathbb{E}_{[\mathbf{x}_p, \mathbf{x}_c, \mathbf{x}_r]^T \sim b} [R([\mathbf{x}_p, \mathbf{x}_c, \mathbf{x}_r]^T, \{\theta_1, \dots, \theta_N\})] \quad h \in [0, H-1]. \quad (16)$$

We solve Eq. (16), which defines multiple, independent, non-convex, constrained optimization problems, using the constrained trust method [TODO: check name] in the `scipy` optimization library for a fixed number of iterations. To evaluate the reward function $R([\mathbf{x}_p, \mathbf{x}_c, \mathbf{x}_r]^\top, \{\theta_1, \dots, \theta_N\})$, we define a trajectory sampler operator $\mathcal{G} : \Theta \rightarrow \mathbb{R}^{3 \times m}$ that takes a trajectory parameter vector as input and produces a set of locations in \mathbb{R}^3 that will be sampled when the robot executes the trajectory, where m is the number of sampled points. These sample points can then be compared with the plume envelope produced by the analytical plume model $f(\mathbf{x}_p, \mathbf{x}_c)$ to count the number of sample points that are contained within the plume envelope.

In practice, we choose our trajectory class to be a lawnmower trajectories (Fig. 2), which were parameterized by a vector θ that determined the origin, orientation, height, width, and resolution of the lawnmower. The trajectory sampler \mathcal{G} produced the lawnmower specified by θ and then subsampled uniformly along its length. We defined the set Θ to enforce that the lawnmower trajectories that were contained within a pre-defined, rectangular safe region and that each lawnmower obeyed a time-based budget constraint.

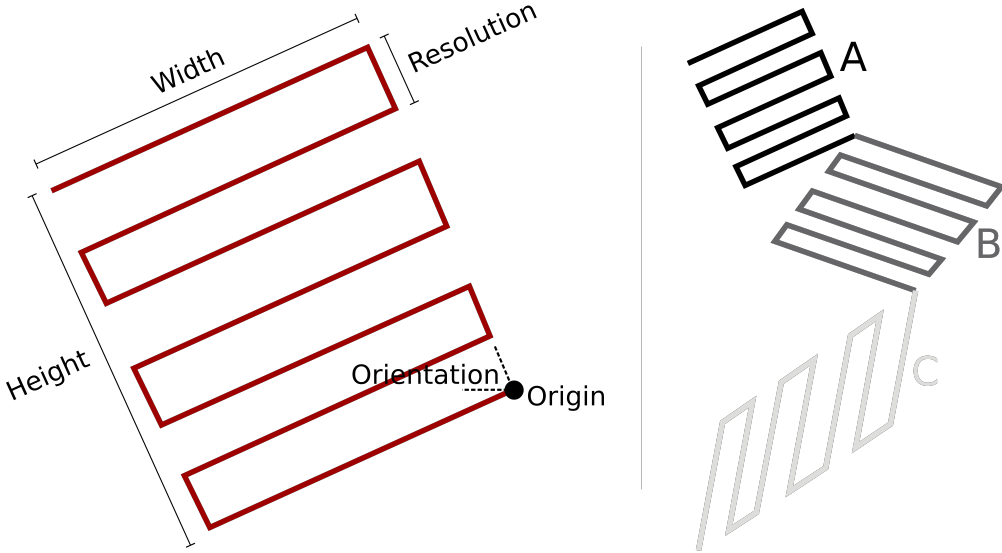


Figure 2: Action space for chained, parameterized lawnmower trajectories. **Left:** the parameterization for a lawnmower, consisting of height, width, orientation, origin, and resolution. **Right:** A chain of three lawnmowers A, B, and C with different parameterizations.

4.4 Iterative Mission Structure

When performing field operations on the research vessel with AUV *Sentry*, we used PHORTEX to enable deployment-by-deployment autonomy that could iteratively improve with each deployment. PHORTEX produces a chained trajectory object, informed by the probabilistic plume forecast. A set of extensive safety checks and human validation steps are subsequently performed on the planned trajectory. The ship is then moved to the deployment point, which is determined by the ship captain based on the planned trajectory and the constraints of other ship operations. *Sentry* was deployed and executed the chained trajectory, collecting scientific sensor observations. Deployments generally lasted 17-20 hours due to battery limitations, after which *Sentry* is recovered by the ship. After recovery, the data collected by *Sentry* is downloaded and used to update PHUMES as in Section 4.2. The updated belief from PHUMES is then used to plan a new chained trajectory, as described in Section 4.3. These belief update and planning steps can take place over several hours (<10 hrs) while the AUV batteries are recharged.

5 Validation in Simulation

[TODO: This section is under significant development; an outline of the intended content is provided.]

- We will first demonstrate PHORTEX within the simulator we've created for generating plume funnels. We will show how PHUMES converges to estimates of the true underlying distributions of initial conditions and parameter settings with and without noise. We will ideally show a graph that is RMSE of params versus mission iteration, and show a steep drop in error with steady improvement as iterations increase (fewer than 10 iterations will be graphed).
- We will additionally show performance on several key metrics, including reward versus iteration, total in-plume samples/accumulated reward under different model settings (e.g., number of samples in PHUMES MCMC chain, prior uncertainty), and model mean and variance with each iteration.
- We will then show how sensitive trajectory optimization settings/chains are to collected reward, intending to show the advantage of using chains over a single highly-resolved lawnmower, at minimum.
- If there is interest/time, we will then show how PHORTEX performs in a numerically realistic simulator (as provided by our collaborator at University of Washington) and compute similar statistics as those indicated above. This addition would be used to demonstrate the complex real-time structure of plume snapshots, and show how the method generalizes to this setting. *VP: note that this is only if there is time; currently planning on only using the field results to demonstrate this, and may save simulation work for later tag-along conference/workshop paper.*

6 Field Deployment

6.1 Cruise Overview

In November 2021, cruise RR2107 aboard the R/V Revelle traveled to the Northern Guaymas Basin in the Gulf of California to study a hydrothermally active ridge (Fig. 3). The cruise mission was two-fold: test novel *in situ* equipment for methane observation, and collect biological samples of microbiota in hydrothermal plume-derived waters for *ex situ* analysis of the structure of the deep plume microbiome. For both of these tasks, placing the autonomous underwater vehicle (AUV) *Sentry* within a moving, evolving black smoker plume was critical, and ideally the location within the plume structure could be determined specifically for later analysis of the microbiological data.

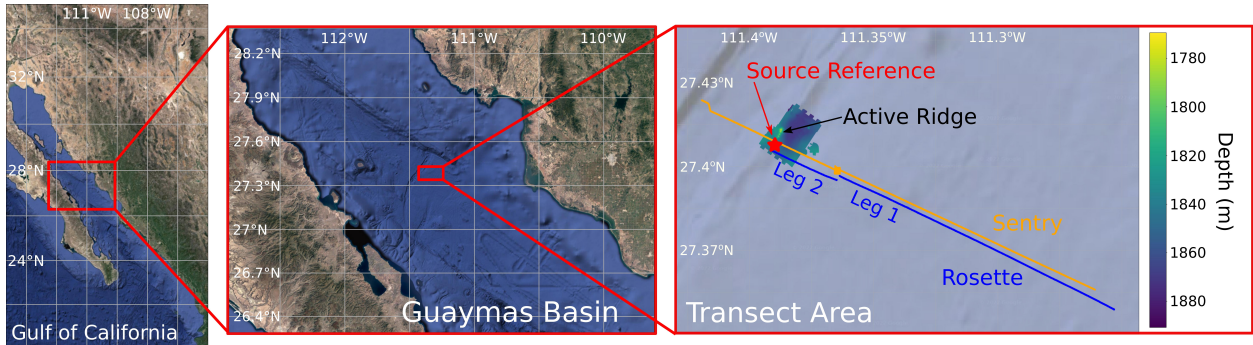


Figure 3: [TODO: this is just a placeholder! An adjusted version of this with better bathy + pictures of the vent from the seafloor + just focused on Sentry lawnmowers will be put here instead. Maps will be preserved for context setting] Located in the northern Guaymas Basin in the Gulf of California, a hydrothermal ridge served as a target for charting mid-water plume structures by AUV *Sentry*.

6.1.1 Site Description

Located approximately 1850 m underwater and at the edge of a graben an additional 300 m deep, the ridge is approximately 600 m long and features several tall sulfide structures 45-75 m in height that demonstrate hydrothermal characteristics. For the purposes of this robotics study, a black smoking chimney at the northernmost point of the

ridge was targeted. Composed of tens of small orifices (<0.1 m diameter) with energetic production of approximately 10 MW each, the smoker at the base is approximately 1.5 m wide, and producing turbid, methane-rich, oxygen-poor turbid fluids heated to 340 °C. The rising “smoke” from the chimney mixes with the background waters, which are generally cold (4 °C), methane-poor, and weakly-stratified (that is, there is a slight density gradient, with the most dense water at the seafloor, and progressively less dense water moving towards the surface). Mixing is driven by advective, diffusive, and reactive processes. Fluid travels from the vent orifice upward through the water column, and is simultaneously horizontally advected by tidally-driven and bathymetrically-affected motion (Fig. 4).

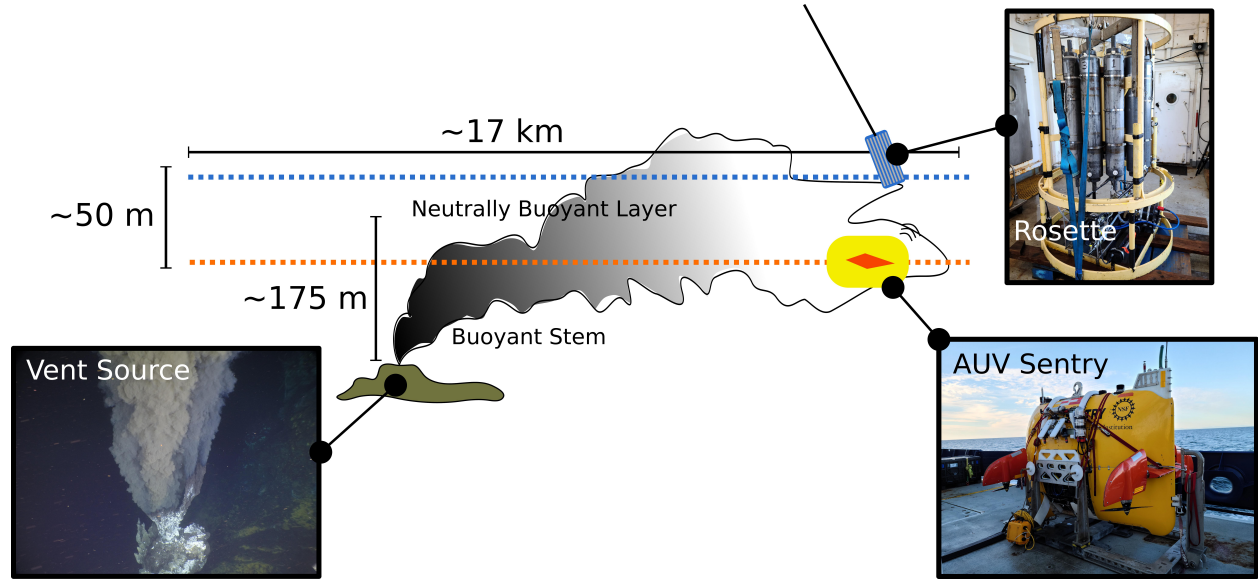


Figure 4: [TODO: this is just a placeholder! An adjusted version of this focused primarily on AUV Sentry will be used instead!] AUV *Sentry* is flown through advecting plumes generated at a hydrothermally active ridge in Guaymas basin.

6.1.2 AUV Sentry and Sensor Interpretation

AUV *Sentry* executes pre-set trajectories (encoded as a set of waypoints) once underway. *Sentry* can be operated in either a depth-hold mode or an altitude-hold mode. The latter is typically used during oceanographic missions. *Sentry* is equipped with ORP, OBS, oxygen, methane, salinity, and temperature sensors, which are logged at 1 Hz on the vehicle. Measurements taken by these instruments were studied in aggregate and used to compute a binary data product, as described in Section 4.1.

6.1.3 Sensors of Opportunity

External to AUV *Sentry* were several core technologies: a winched rosette, a tiltmeter, and ROV *JASON*. These were “sensors of opportunity” for the *Sentry* operations, and yielded information that we leveraged within PHORTEX (particularly PHUMES) for more accurate forecasting.

A rosette is a metal frame on which standard oceanographic sensing equipment (e.g., conductivity-temperature-depth probe) and Niskin bottle containers are mounted. A rosette is typically cast over the side of a ship and used to collect a vertical profile of sensing targets and collect water samples for *ex situ* analysis. We used profiles of temperature and salinity collected in this manner to generate a salinity-temperature-density curve that was used within PHUMES modeling [TODO: add a figure showing these profiles + model fit].

A tiltmeter is anchored to the bottom of a water body and measures advective crossflow magnitude and direction. A tiltmeter was mounted at various locations over several days during the expedition [TODO: get location] and

deployed for [TODO: number of hours]. This data was used to generate an estimate of the temporal crossflow function utilized in PHUMES. It was observed that this current function was periodic, largely driven by tidal structure in the basin [TODO: make a figure showing the data and model].

Finally, ROV *JASON* is a remotely piloted vehicle, and was used to make visual and instrumented observations of the vents that produce the plumes to be studied by *Sentry*. Direct measurements of vent temperature, and estimates of vent area and exit velocity were used to center prior distributions over model parameters in PHUMES [TODO: maybe insert a table with some of these core measurements?].

6.2 Experimental Results

[TODO: Note that this section is under construction! An overview of what this section will entail is below!]

- This section will primarily present 4 trials that we performed while at sea – 1 designed completely by hand, 2 partially designed by a person and by PHORTEX, and one completely designed by PHORTEX. The intent is to show the “planning spectrum” from fully-human to fully algorithmic, and comment on the form of these plans and their relative efficacy. Note that because the conditions between each iteration are different, the iterations are themselves not necessarily directly comparable (as in, claiming that one is “better” than another may be...bold) so we will be primarily focused on general metrics across all dives.
- The Planning Spectrum:
 - We will show each of the 4 dives from fully human-designed to fully algorithmically designed. We will point out how the form factor between the lawnmowers/lawnmower chains differ, highlighting in particular how algorithmic chains tend to be strongly impacted by estimated crossflow, causing the trajectories to “fan” out; whereas human design trajectories tend to be conservatively placed centered at a known source.
 - We will show each of the four dives in both space and time; this will allow us to mark-up the figures and show where and when detections were made. We will ideally show that algorithmic trajectories tend to have more evenly distributed detections throughout a dive. We will also hopefully show that algorithmic trajectories tend to have more “far afield” positive detections of plumes.
- Quantitative Results:
 - Some quantitative results we will share for each dive will include proportion of total samples in plume, proportion of total samples within/outside a certain radius from a known vent, RMSE of estimates vent characteristics by PHUMES (train a naive PHUMES model from observations collected by each dive, how to the dives inter-compare? How does it compare with estimates from ROV *JASON*? How does a per-dive iteration look?)

7 Discussion

[TODO: Note that this section is still under heavy construction, pending results! Drafty remarks below!]

PHORTEX is a method that leverages physically-informed structures in order to grapple with the extreme partial observability of the expeditionary science problem in spatiotemporal environments, and presents a flexible trajectory optimization which generates trajectories that honor both robotic and operational constraints. Practically, PHORTEX is enabled by the need for a “practical time” algorithmic framework to assist with decision-making on a deployment-by-deployment basis. This is in direct contrast with many state-of-the-art informative path planning frameworks which primarily focus on underway autonomous systems. While the future of expeditionary science will increasingly demand robotic platforms that can perform such underway capabilities, PHORTEX is well suited as a bridge that brings intelligence capacities to existing and pervasive expeditionary infrastructure with easily scaled, modular, and supervisory features.

In both simulation and field trials for hydrothermal plume charting, we demonstrated that PHORTEX with binary pseudo-sensor, PHUMES model, and chained, open-loop trajectory handler was able to [TODO: pithy statement about tangible results here]. The modular framework can be easily adapted to other spatiotemporal tasks. The binary pseudo-sensor could be replaced with a continuous observation measurement from a sensor, or other continuous signal. The scientific model leveraged within PHUMES could be trivially swapped for any other ODE or simplified PDE system, which could be well suited to ecological/population studies, fluidic or thermal transport, or materials design. The reward function, action primitive, and trajectory optimization technique could further be selected based on domain requirements.

8 Future Work

There is a significant desire for embodied intelligence and assistive decision-making infrastructure for environmental exploration and expeditionary science. PHORTEX is an autonomy stack that has been demonstrated at-scale for a deployment-by-deployment mission design task for deep sea hydrothermal plume charting, and showed quantitative gains over typical exploration strategies while also fitting directly into the operational ecosystem of a ship at sea. Future work will push aspects of PHORTEX further, particularly focusing on adding sophistication to PHUMES spatiotemporal modeling from partial observations, increasing underway autonomy capabilities, and demonstrating improved scientific outcomes with this infrastructure.

8.1 Open Challenges

VP: note that this section is currently pulled from our RLDM piece, and will need some serious editing for brevity and to improve citation.

A number of open challenges in representation learning and decision-making in the context of expeditionary robotics remain. Briefly, several key areas we see as open opportunities are outlined here.

8.1.1 Belief Representation

Heterogeneous observation models: Robots used in environmental studies typically carry heterogeneous observational equipment (e.g., point sensors, cameras, acoustic sonar). Optimizing sample collection to address scientific hypotheses requires fusing these different sensing modalities together and implementing complex observational models that link domain knowledge about sensor data to the state of a scientific phenomenon. Embedding expert knowledge into fused observational models, modeling sensor importance to a particular task, and reasoning across different sensors with distinct spatial and temporal resolutions (e.g., [Sarkar et al., 2014]) are all active challenges.

Epistemic and aleatoric uncertainty: Reducing epistemic uncertainty of a spatiotemporal environment requires access to a model of the underlying dynamical system, or a data-driven technique that can uncover it. Extracting physically-meaningful quantities from observational data is typically performed post-expedition using computationally expensive numerical models “tuned” by observations. While this lends itself well to Bayesian inference formulations, it is intractable for practical decision-making. Data-driven techniques for model discovery [Raissi et al., 2019] may be arguably more tractable, but generally suffer small-data challenges. Developing models that overcome the challenges of efficiently characterizing spatiotemporal dynamics from streaming, sparse observations would generally improve expeditionary robotics. Additionally, there is a unique opportunity to enable computation of proxies for aleatoric uncertainty, which are well-described in spatiotemporal environments with measures of chaotic motion (e.g., Lyapunov exponents) inferred from data [Blanchard and Sapsis, 2019]. The implication that aleatoric uncertainty can be estimated has yet to be utilized to, e.g., assess the attainable resolution of a model or set planning horizons.

Scientific knowledge as inductive bias: The kernel of a GP, the loss function in a neural network, or the activation functions between layers in a deep network can all be viewed as forms of inductive bias in a learning problem. For data-driven discovery of spatiotemporal dynamics, improving sample efficiency by leveraging opportunities to

inject scientific knowledge to alleviate the learning burden is an open problem. While canonical numerical models of spatiotemporal phenomena are too computationally expensive to directly incorporate into e.g., GP kernels, the physical principles that underlie these models can be more easily summarized. “Physically-informed” data-driven probabilistic representations have been demonstrated outside of expeditionary robotics [Raissi et al., 2019] and some work within IPP [Salam and Hsieh, 2019] shows rich opportunities for analyzing and extending these methods for larger environments and longer planning horizons.

Low-dimensional state embeddings: Expressing a spatiotemporal environment completely would require an exceedingly large, high-dimensional representation. Model order reduction (MOR) techniques reduce the dimensionality of spatiotemporal systems to a set of weights and vectors that sufficiently describe patterns in the dynamics. Uncovering low-dimensional state embeddings from partially-observed expedition data is a general challenge; uncovering a *useful* embedding for a specific decision-making problem is additionally challenging. Access to such an embedding would reduce the computational burden of representing belief in large environments for planning.

8.1.2 Decision-Making

Rollout-based planning with expensive belief models: State-of-the-art planners for POMDP problems often make use of rollout-based planning in tree search frameworks; continuous search variables are handled using strategies such as progressive widening or scenario sampling [Sunberg and Kochenderfer, 2018]. However, these planners require extensive online simulations for each rollout performed. Forward-simulating the dynamics and observational models for complex, spatiotemporal phenomena can be computationally intensive, which often limits the feasible look-ahead horizon in real-time operations on computationally-limited robotic platforms. Planners that selectively or adaptively perform expensive rollouts, automatically adjust the planning horizon based on the dynamics of the environmental system, or make use of continuous, offline planners would enable improved decision-making for expeditionary science.

Abstractions for planning: Another promising direction is the development of abstract planning domains for expeditionary robotic problems. Instead of planning over a set of low-level, continuous control actions, planners could make use of high-level, abstract actions. These planning abstractions may come from human scientists or could be learned directly using recent developments in reinforcement learning and macro-action discovery [Flaspohler et al., 2020].

Information rewards and task-driven exploration: Due to partial observability and stochastic dynamics in spatiotemporal contexts, a decision-maker must operate with significant and often growing state uncertainty. However, not all state uncertainty impacts task performance and uniform information gathering strategies can be inefficient. Understanding the value of information for accomplishing a task is a known challenge for planning under uncertainty and this is particularly true for expeditionary robotics. Recent works that develop heuristic information rewards [Flaspohler et al., 2019] or task-driven value of information metrics [Flaspohler et al., 2020] begin to build the tools necessary for expeditionary robotic planning.

Robust planning under model mismatch and uncertainty: Scientific models, whether data-driven or based on physical principles, are always imperfect representations of a robot’s environment. Model mismatch or uncertainty in key model parameters leads to discrepancies between the environmental predictions that a robot uses during planning and its real-time observations. Planning robot trajectories that entirely miss a phenomenon due to overconfidence in an incorrect model is detrimental to scientific objectives. Planners must develop policies or trajectories that are robust to model mismatch and uncertainty, or are guaranteed to perform as well as a simple, naive data collection strategy.

Interpretable and operational decision-making: Decision-making algorithms must interface with and are constrained by a variety of stakeholders, including scientists, robot operators, and engineers. For example, when deploying an AUV from an oceanographic research vessel, the decision-making algorithm must account for ship scheduling, timing delays, weather, and multi-vehicle operations. This requires developing flexible planners that can understand and account for these complex constraints. Additionally, stakeholders are often concerned with robot safety and data quality. Producing plans that are interpretable for scientific and operational stakeholders is key for building trust and confidence in scientific autonomy.

8.2 Improving Human Decision-Making Capabilities

PHORTEX fundamentally relies on human expertise to inform the scientific models used within PHUMES, generate useful reward functions, set trajectory primitives, and operationally get deployed on a robotic platform while in the field. Relieving the burden on these human agents—whether by creating aggregated data products or proposing multiple field missions with explanations—could lead to significant gains in the short-terms for expeditionary science tasks. On this research cruise, we created data displays for AUV *Sentry* that displayed real-time science data reported every 2 min via acoustic modem from the vehicle. While a significantly limited subset of the data, this real-time reporting was sufficient for real-time anomaly discovery by human watchstanders. This capability, which to many academic and industrial roboticists may seem obvious or straightforward, is not yet pervasive or standard in the sciences or among scientific instruments on state-of-the-art vessels or autonomous platforms. Attention paid towards improving data infrastructure, data visualization, real-time signal processing, and operational training could go a long way.

9 Conclusion

In this paper, we presented PHORTEX:PHysically-informed Open-loop Robotic Trajectories for EXpeditions, composed of a probabilistic model that embedded a simplified scientific summary to enable sample-efficiency belief representation learning (PHUMES) and a trajectory optimizer that chained open-loop trajectory primitives into missions that respected severe operational constraints for practical field experiments. PHORTEX was deployed at-scale in the field for deep sea hydrothermal plume charting, in which we demonstrated in the field that [TODO: pithy results summary]. In simulation, we showed that [TODO: pithy sim results summary].

Environmental exploration is a pressing societal challenge, and algorithmic development in service of expeditionary science presents many compelling technical opportunities in representation learning and decision-making for both deployment-by-deployment and underway autonomous systems. [TODO: further looking ahead statement]

Acknowledgments

Funding sources were BLAH. Many thanks to the Captain and crew of R/V *Revelle*, Sentry team engineers, and Jason team engineers who make expeditionary science possible, particularly S. Kelley, Z. Berkowitz, S. Suman, A. Sutherland, J. Fujii, J. Garcia, for their extensive help before and during sea trials with AUV *Sentry*. Additional thanks to M. Jakuba, C. German, J. Kapit, W. Pardis, B. Colson, S. Youngs, X. Zhang, G. Xu, T. Barreyre, D. Martello, C. Cenedese, and D. Fornari for their support (engineering and professional), insights, and conversations.

References

- Agrawal, R. (1995). Sample mean based index policies by $O(\log n)$ regret for the multi-armed bandit problem. *Adv. Appl. Probab.*, 27(4):1054–1078.
- Arora, A., Furlong, P. M., Fitch, R., Sukkarieh, S., and Fong, T. (2017). Multi-modal active perception for information gathering in science missions. In *Proc. Int. Symp. Auton. Robots*, pages 1–27.
- Auer, P. (2002). Using confidence bounds for exploitation-exploration trade-offs. *J. Mach. Learn. Research*, 3(Nov):397–422.
- Beaulieu, S. E., Baker, E. T., and German, C. R. (2015). Where are the undiscovered hydrothermal vents on oceanic spreading ridges? *Deep Sea Research Part II: Topical Studies in Oceanography*, 121:202–212.
- Binney, J. and Sukhatme, G. S. (2012). Branch and bound for informative path planning. In *Proc. IEEE Int. Conf. Robot. Autom.*, pages 2147–2154.

- Blanchard, A. and Sapsis, T. P. (2019). Analytical description of optimally time-dependent modes for reduced-order modeling of transient instabilities. *SIAM Journal on Applied Dynamical Systems*, 18(2):1143–1162.
- Branch, A., McMahon, J., Xu, G., Jakuba, M. V., German, C. R., Chien, S., Kinsey, J. C., Bowen, A. D., Hand, K. P., and Seewald, J. S. (2020). Demonstration of autonomous nested search for local maxima using an unmanned underwater vehicle. In *2020 IEEE International Conference on Robotics and Automation (ICRA)*, pages 1888–1895. IEEE.
- Browne, C. B., Powley, E., Whitehouse, D., Lucas, S. M., Cowling, P. I., Rohlfschagen, P., Tavener, S., Perez, D., Samothrakis, S., and Colton, S. (2012). A survey of Monte Carlo tree search methods. *IEEE Trans. Comput. Intell. AI Games*, 4(1):1–43.
- Camilli, R., Reddy, C. M., Yoerger, D. R., Van Mooy, B. A., Jakuba, M. V., Kinsey, J. C., McIntyre, C. P., Sylva, S. P., and Maloney, J. V. (2010). Tracking hydrocarbon plume transport and biodegradation at deepwater horizon. *Science*, 330(6001):201–204.
- Chen, X.-x. and Huang, J. (2019). Odor source localization algorithms on mobile robots: A review and future outlook. *Robotics and Autonomous Systems*, 112:123–136.
- Chevaldonné, P., Desbruyères, D., and Le Haître, M. (1991). Time-series of temperature from three deep-sea hydrothermal vent sites. *Deep Sea Research Part A. Oceanographic Research Papers*, 38(11):1417–1430.
- Corliss, J. B., Dymond, J., Gordon, L. I., Edmond, J. M., von Herzen, R. P., Ballard, R. D., Green, K., Williams, D., Bainbridge, A., Crane, K., et al. (1979). Submarine thermal springs on the galapagos rift. *Science*, 203(4385):1073–1083.
- Edwards, P. N. (2001). *Representing the global atmosphere: Computer models, data, and knowledge about climate change*, volume 1. MIT Press Cambridge, MA.
- Ferri, G., Jakuba, M. V., and Yoerger, D. R. (2010). A novel trigger-based method for hydrothermal vents prospecting using an autonomous underwater robot. *Autonomous Robots*, 29(1):67–83.
- Flaspohler, G., Preston, V., Michel, A. P., Girdhar, Y., and Roy, N. (2019). Information-guided robotic maximum seek-and-sample in partially observable continuous environments. *IEEE Robotics and Automation Letters*, pages 3782–3789.
- Flaspohler, G., Roy, N. A., and Fisher III, J. W. (2020). Belief-dependent macro-action discovery in POMDPs using the value of information. *Advances in Neural Information Processing Systems*, 33:11108–11118.
- Garg, S., Singh, A., and Ramos, F. (2012). Learning non-stationary space-time models for environmental monitoring. In *Twenty-Sixth AAAI Conference on Artificial Intelligence*.
- Green, A., Singhal, R., and Venkateswar, R. (1980). Analytic extensions of the gaussian plume model. *Journal of the Air Pollution Control Association*, 30(7):773–776.
- Green, P. J. (1995). Reversible jump Markov chain Monte Carlo computation and Bayesian model determination. *Biometrika*, 82(4):711–732.
- Hennig, P. and Schuler, C. J. (2012). Entropy search for information-efficient global optimization. *J. Mach. Learn. Res.*, 13(Jun):1809–1837.
- Hernández-Lobato, J. M., Hoffman, M. W., and Ghahramani, Z. (2014). Predictive entropy search for efficient global optimization of black-box functions. In *Proc. 27th Int. Conf. Neural Inf. Process. Syst.*, pages 918–926.
- Hitz, G., Galceran, E., Garneau, M.-È., Pomerleau, F., and Siegwart, R. (2017). Adaptive continuous-space informative path planning for online environmental monitoring. *J. Field Robot.*, 34(8):1427–1449.
- Jakuba, M. V. (2007). *Stochastic mapping for chemical plume source localization with application to autonomous hydrothermal vent discovery*. PhD thesis, Massachusetts Institute of Technology.

- Jannasch, H. W. and Mottl, M. J. (1985). Geomicrobiology of deep-sea hydrothermal vents. *Science*, 229(4715):717–725.
- Jawaid, S. T. and Smith, S. L. (2015). Informative path planning as a maximum traveling salesman problem with submodular rewards. *Discr. Appl. Math.*, 186:112–127.
- Jones, D. R., Schonlau, M., and Welch, W. J. (1998). Efficient global optimization of expensive black-box functions. *J. Global Optim.*, 13(4):455–492.
- Kaiser, C. L., Yoerger, D. R., Kinsey, J. C., Kelley, S., Billings, A., Fujii, J., Suman, S., Jakuba, M., Berkowitz, Z., German, C. R., et al. (2016). The design and 200 day per year operation of the autonomous underwater vehicle sentry. In *2016 IEEE/OES Autonomous Underwater Vehicles (AUV)*, pages 251–260. IEEE.
- Kim, J., Son, S.-K., Kim, D., Pak, S.-J., Yu, O. H., Walker, S. L., Oh, J., Choi, S. K., Ra, K., Ko, Y., et al. (2020). Discovery of active hydrothermal vent fields along the central indian ridge, 8–12 s. *Geochemistry, Geophysics, Geosystems*, 21(8):e2020GC009058.
- Krause, A., Singh, A., and Guestrin, C. (2008a). Near-optimal sensor placements in Gaussian processes: Theory, efficient algorithms and empirical studies. *Journal of Machine Learning Research*, 9(2).
- Krause, A., Singh, A., and Guestrin, C. (2008b). Near-Optimal Sensor Placements in Gaussian Processes: Theory, Efficient Algorithms and Empirical Studies. *J. Mach. Learn. Res.*, 9:235–284.
- Kushner, H. J. (1964). A new method of locating the maximum point of an arbitrary multipeak curve in the presence of noise. *J. Basic Eng.*, 86(1):97–106.
- Lavelle, J., Di Iorio, D., and Rona, P. (2013). A turbulent convection model with an observational context for a deep-sea hydrothermal plume in a time-variable cross flow. *Journal of Geophysical Research: Oceans*, 118(11):6145–6160.
- Li, S., Guo, Y., and Bingham, B. (2014). Multi-robot cooperative control for monitoring and tracking dynamic plumes. In *2014 IEEE International Conference on Robotics and Automation (ICRA)*, pages 67–73. IEEE.
- Lim, Z. W., Hsu, D., and Lee, W. S. (2016). Adaptive informative path planning in metric spaces. *Int. J. Robot. Res.*, 35(5):585–598.
- Ludwig, F., Gasiorek, L., and Ruff, R. (1977). Simplification of a gaussian puff model for real-time minicomputer use. *Atmospheric Environment* (1967), 11(5):431–436.
- MacKay, D. J. (1998). Introduction to Monte Carlo methods. In *Learning in graphical models*, pages 175–204. Springer.
- Marchant, R., Ramos, F., and Sanner, S. (2014). Sequential Bayesian optimisation for spatial-temporal monitoring. In *Proc. 13th Conf. Uncertainty Artif. Intell.*, pages 553–562.
- Martin, W., Baross, J., Kelley, D., and Russell, M. J. (2008). Hydrothermal vents and the origin of life. *Nature Reviews Microbiology*, 6(11):805–814.
- Mason, J. C., Branch, A., Xu, G., Jakuba, M. V., German, C. R., Chien, S., Bowen, A. D., Hand, K. P., and Seewald, J. S. (2020). Evaluation of auv search strategies for the localization of hydrothermal venting.
- Mcgill, K. and Taylor, S. (2011). Robot algorithms for localization of multiple emission sources. *ACM Computing Surveys (CSUR)*, 43(3):1–25.
- Metropolis, N., Rosenbluth, A. W., Rosenbluth, M. N., Teller, A. H., and Teller, E. (1953). Equation of state calculations by fast computing machines. *The journal of chemical physics*, 21(6):1087–1092.
- Morse, T. M., Lockery, S. R., and Ferrée, T. C. (1998). Robust spatial navigation in a robot inspired by chemotaxis in *caenorhabditis elegans*. *Adaptive Behavior*, 6(3-4):393–410.

- Morton, B., Taylor, G. I., and Turner, J. S. (1956). Turbulent gravitational convection from maintained and instantaneous sources. *Proceedings of the Royal Society of London. Series A. Mathematical and Physical Sciences*, pages 1–23.
- Nakamura, K., Toki, T., Mochizuki, N., Asada, M., Ishibashi, J.-i., Nogi, Y., Yoshikawa, S., Miyazaki, J.-i., and Okino, K. (2013). Discovery of a new hydrothermal vent based on an underwater, high-resolution geophysical survey. *Deep Sea Research Part I: Oceanographic Research Papers*, 74:1–10.
- Neal, R. M. et al. (2011). MCMC using Hamiltonian dynamics. *Handbook of Markov chain Monte Carlo*, pages 113–162.
- Nemhauser, G. L., Wolsey, L. A., and Fisher, M. L. (1978). An analysis of approximations for maximizing submodular set functions—i. *Math. Program.*, 14(1):265–294.
- Paduan, J. B., Zierenberg, R. A., Clague, D. A., Spelz, R. M., Caress, D. W., Troni, G., Thomas, H., Glessner, J., Lilley, M. D., Lorenson, T., et al. (2018). Discovery of hydrothermal vent fields on alarcón rise and in southern pescadero basin, gulf of california. *Geochemistry, Geophysics, Geosystems*, 19(12):4788–4819.
- Peng, L., Lipinski, D., and Mohseni, K. (2014). Dynamic data driven application system for plume estimation using uavs. *Journal of Intelligent & Robotic Systems*, 74(1):421–436.
- Raissi, M., Perdikaris, P., and Karniadakis, G. E. (2019). Physics-informed neural networks: A deep learning framework for solving forward and inverse problems involving nonlinear partial differential equations. *Journal of Computational Physics*, 378:686–707.
- Reddy, G., Murthy, V. N., and Vergassola, M. (2022). Olfactory sensing and navigation in turbulent environments. *Annual Review of Condensed Matter Physics*, 13.
- Salam, T. and Hsieh, M. A. (2019). Adaptive sampling and reduced-order modeling of dynamic processes by robot teams. *IEEE Robotics and Automation Letters*, 4(2):477–484.
- Sarkar, S., Sarkar, S., Virani, N., Ray, A., and Yasar, M. (2014). Sensor fusion for fault detection and classification in distributed physical processes. *Frontiers in Robotics and AI*, 1:16.
- Särkkä, S. (2013). *Bayesian filtering and smoothing*. Number 3. Cambridge university press.
- Silver, D. and Veness, J. (2010). Monte-Carlo planning in large POMDPs. In *Proc. Adv. Neural Inf. Process. Syst.*, pages 2164–2172.
- Singh, A., Krause, A., and Kaiser, W. J. (2009). Nonmyopic adaptive informative path planning for multiple robots. In *Proc. 21st Int. Joint Conf. Artif Intell.*, pages 1843–1850.
- Snoek, J., Larochelle, H., and Adams, R. P. (2012). Practical Bayesian optimization of machine learning algorithms. In *Proc. Adv. Neural Info. Process. Syst.*, pages 2951–2959.
- Speer, K. G. and Rona, P. A. (1989). A model of an atlantic and pacific hydrothermal plume. *Journal of Geophysical Research: Oceans*, 94(C5):6213–6220.
- Srinivas, N., Krause, A., Kakade, S. M., and Seeger, M. W. (2012). Information-Theoretic Regret Bounds for Gaussian Process Optimization in the Bandit Setting. *IEEE Trans. Inf. Theory*, 58:3250–3265.
- Sunberg, Z. N. and Kochenderfer, M. J. (2018). Online algorithms for POMDPs with continuous state, action, and observation spaces. In *Proc. 24th Int. Conf. Automated Plan. Schedul.*
- Tohidi, A. and Kaye, N. B. (2016). Highly buoyant bent-over plumes in a boundary layer. *Atmospheric Environment*, 131:97–114.
- Vergassola, M., Villermaux, E., and Shraiman, B. I. (2007). ‘infotaxis’ as a strategy for searching without gradients. *Nature*, 445(7126):406–409.

Wang, L., Pang, S., and Xu, G. (2020). 3-dimensional hydrothermal vent localization based on chemical plume tracing. In *Global Oceans 2020: Singapore–US Gulf Coast*, pages 1–7. IEEE.

Welch, G., Bishop, G., et al. (1995). An introduction to the kalman filter.

Xu, G. and Di Iorio, D. (2012). Deep sea hydrothermal plumes and their interaction with oscillatory flows. *Geochemistry, Geophysics, Geosystems*, 13(9).